Frontiers in Bioscience Landmark

Front. Biosci. (Landmark Ed) **2026**; 31(10): 54785
https://doi.org/10.31083/FBL54785

Original Research

Iguratimod Modulates M1 Macrophage Polarization Via the NOTCH4–KLF4 Axis to Alleviate Antibody-Mediated Rejection

Zhou Hang[1,†], Junqi Zhang[1,†], Chengcheng Yang[1], Ming Zheng[1], Zexin Yang[1], Jie Xu[1], Peng Han[2,*], Min Gu[1,*]

[1]Department of Urology, Jiangsu Key Laboratory of Urological Disease Prevention and Treatment, The Second Affiliated Hospital of Nanjing Medical University, Nanjing Medical University, 210008 Nanjing, Jiangsu, China
[2]Department of Urology, The First Affiliated Hospital of Nanjing Medical University, Nanjing Medical University, 210008 Nanjing, Jiangsu, China
*Correspondence: hanpeng2015@njmu.edu.com (Peng Han); njmuwzj1990@hotmail.com (Min Gu)
[†]These authors contributed equally.
Academic Editor: Guoping Zheng
Submitted: 11 June 2026 Revised: 11 August 2026 Accepted: 18 August 2026 Published: 30 September 2026

Abstract

Background: Iguratimod (IGT) is a small-molecule anti-inflammatory agent that effectively attenuates the progression of antibody-mediated rejection (ABMR). However, the underlying mechanism of action of IGT remains poorly understood. Thus, this study aimed to investigate the mechanism through which IGT regulates macrophage polarization and ABMR. **Methods:** A mouse model of ABMR was established by performing kidney transplantation after skin graft-induced sensitization. Experimental interventions included neurogenic locus notch homolog protein 4 (NOTCH4) knockout mice and oral administration of IGT. RNA sequencing, quantitative polymerase chain reaction, Western blotting (WB), flow cytometry, and immunofluorescence (IF) staining were performed to investigate M1 macrophage polarization and the Jagged1–NOTCH4 signaling pathway. **Results:** This study found that IGT significantly reduced M1 macrophage infiltration into renal allografts in a mouse model of ABMR. Transcriptomic sequencing and subsequent biological experiments indicated that IGT may regulate macrophage polarization through the Jagged1–NOTCH4 pathway. **Conclusion:** M1 macrophage polarization may contribute to the initiation and progression of ABMR following kidney transplantation. IGT attenuates M1 macrophage polarization by inhibiting Jagged1–NOTCH4–Krüppel-like Factor 4 (KLF4) signaling.

Keywords: kidney transplantation; graft rejection; macrophage activation; iguratimod; Notch

1. Introduction

Kidney transplantation is the most effective treatment for end-stage renal disease, significantly prolonging patient survival and improving patients' quality of life [1]. Depending on the underlying mechanism, rejection episodes after transplantation can be classified as T cell-mediated rejection (TCMR) or antibody-mediated rejection (ABMR) [2]. Multiple studies have confirmed that ABMR is closely associated with long-term graft failure [3,4].

During allograft rejection, the extent of monocyte/macrophage infiltration within the graft correlates with the severity of tissue injury and graft outcome [5,6]. Monocytes/macrophages can modify their phenotype and function in response to changes in the local microenvironment, a process termed macrophage polarization [7]. After infiltrating grafts affected by ABMR, monocytes/macrophages may acquire proinflammatory phenotypes that exacerbate antibody-mediated graft injury and rejection [8]. Recent research has revealed that circulating immune cells exert substantial effects on the function of various organs [9,10]. The gut microbiota and associated metabolites also influence the immunological microenvironment of the graft, thereby affecting graft rejection and survival [11]. However, the precise molecular mechanisms underlying macrophage activation within the graft remain unclear.

NOTCH1–4 are highly conserved transmembrane receptors that are widely expressed in mammalian cells and participate in diverse physiological and pathological processes [12,13]. Ligand binding triggers proteolytic cleavage of the neurogenic locus notch homolog protein (NOTCH) receptor, releasing the NOTCH intracellular domain (NICD). The NICD subsequently translocates to the nucleus, where it interacts with recombination signal-binding protein for immunoglobulin kappa J region (RBPJ) to form a transcriptional coactivator complex that regulates target-gene expression.

Iguratimod (IGT) is a small-molecule anti-inflammatory drug that has been widely used to treat rheumatoid arthritis because of its potent ability to inhibit cytokine-mediated inflammatory responses [14]. Previous studies have confirmed that IGT delays renal damage in mouse models of lupus nephritis by suppressing antibody-mediated immune responses [15]. More importantly, our previous clinical studies of IGT in transplantation demonstrated that its combination with conventional immunosuppressants reduced the incidence of post-transplant rejection [16,17]. Our earlier study also revealed that, in a

Copyright: © 2026 The Author(s). Published by IMR Press.
This is an open access article under the CC BY 4.0 license.

Publisher's Note: IMR Press stays neutral with regard to jurisdictional claims in published maps and institutional affiliations.

rat kidney transplantation model, IGT attenuated ABMR and reduced renal injury [18]. Nevertheless, the precise mechanism of action of IGT remains unclear.

In this study, we demonstrated that IGT suppresses the proinflammatory phenotype of macrophages in renal allografts affected by ABMR and that its anti-inflammatory effects are associated with the NOTCH signaling pathway. Thus, we hypothesized that IGT may inhibit M1 macrophage polarization through the NOTCH4/Hairy and Enhancer of Split 1 (HES1)/Krüppel-like Factor 4 (KLF4) pathway, thereby improving the function of renal allografts affected by ABMR. Collectively, these findings elucidate the regulatory mechanism of IGT and highlight the critical role of the NOTCH4/HES1/KLF4 axis in macrophage activation during IGT-mediated alleviation of ABMR.

2. Methods

2.1 Mice

Adult male C57BL/6 and BALB/c mice weighing 20–25 g were obtained from the Animal Core Facility of Nanjing Medical University, Nanjing, China, and used as recipients and donors, respectively. NOTCH4-knockout C57BL/6 mice were purchased from Shanghai Model Organisms Center, Inc. The study was carried out in accordance with the Animal Research: Reporting of In Vivo Experiments (ARRIVE guidelines). All animal experiments were conducted in accordance with the Guide for the Care and Use of Laboratory Animals and the institutional guidelines of the Nanjing Medical University Institutional Ethical Guidelines for animal experiments (approval no. IACUC-2109025). In this study, separate sample sizes were used for different readouts: n = 5 mice per group for histopathological staining and banff scoring, and n = 3 mice per group for immunofluorescence staining and flow cytometry assays. Male C57BL/6 and BALB/c mice aged 8–10 weeks with body weight of 20–25 g were included. Animals that died within 72 h after transplantation due to surgical complications or exhibited anastomotic failure were excluded from analysis. Mice were randomly allocated to experimental groups by simple random sampling before surgery. The researcher performing histopathological evaluation and C3d immunofluorescence semiquantitative scoring was blinded to group assignments.

2.2 Allogeneic Mouse ABMR Model

Full-thickness skin grafts measuring 0.8–1.0 cm × 1.0 cm were harvested from the backs of BALB/c donor mice and transplanted onto the backs of C57BL/6 recipient mice. Five days after skin grafting for presensitization, kidney grafts were harvested from BALB/c mice. The renal artery and vein were anastomosed end-to-side to the aorta and inferior vena cava of the C57BL/6 recipients, respectively. The graft ureter was anastomosed to the recipient bladder. Oral administration of IGT (S5648, Selleck, Houston, Texas, USA) at 35 mg/kg/day was initiated on the day of skin grafting. Acute ABMR in the mouse renal allografts was diagnosed according to the Banff 2019 criteria. During surgery, mice were anesthetized by inhalation with isoflurane (R510-22-10, RWD Life Science Co. Shenzhen, Guangdong, China), with 3% used for induction and approximately 1.5% for maintenance [19]. The anesthetic concentration was adjusted as necessary according to the animals' responses. Mice were euthanized by cervical dislocation under deep anesthesia. Cervical dislocation was performed by trained personnel only after confirming a sufficient depth of anesthesia, as evidenced by the absence of the righting reflex and response to noxious stimuli. Death was confirmed by the cessation of respiration and heartbeat, together with the absence of reflexes.

The experimental groups were as follows. Syngeneic (SYN) group: C57BL/6 mice were used as both donors and recipients to establish SYN kidney grafts. ABMR group: BALB/c mice were used as donors, and presensitized C57BL/6 mice were used as recipients. IGT group: BALB/c mice were used as donors, and presensitized C57BL/6 mice were used as recipients; recipient mice concurrently received IGT treatment.

2.3 Histology

On day 5 after kidney transplantation, the renal allografts were harvested, fixed in formalin, embedded in paraffin, and sectioned. Tissue sections were stained with hematoxylin and eosin (H&E) and periodic acid-Schiff (PAS).

C3d deposition was detected by immunofluorescence (IF) staining. Frozen kidney sections were fixed in acetone, blocked with blocking buffer (P0260, Beyotime, Shanghai, China), and incubated overnight at 4 °C with an anti-C3d antibody (5 µg/ml, AF2655-SP, R&D Systems, Minneapolis, MN, USA). The sections were subsequently incubated with a Cy3-conjugated secondary antibody (1:500, A0507, Beyotime, Shanghai, China). C3d complement deposition was separately evaluated by a semiquantitative scoring protocol established in rodent kidney allograft models [20].

2.4 Isolation, Culture, and Treatment of Bone Marrow-Derived Macrophages (BMDMs)

BMDMs were isolated from the femurs and tibias of BALB/c mice, purified by density-gradient centrifugation, and cultured in Dulbecco's modified Eagle medium (DMEM) supplemented with 10% fetal bovine serum, 1% antibiotics, and macrophage colony-stimulating factor (M-CSF; 30 ng/mL). After 7 days of differentiation, mature BMDMs were treated for 24 h with M-CSF alone (M0), M-CSF plus lipopolysaccharide/interferon-γ (LPS/IFN-γ; M1), or M-CSF plus LPS/IFN-γ and IGT (10 µg/mL) before subsequent experiments. All cell lines were validated by Short Tandem Repeat (STR) profiling and tested negative for mycoplasma.

2.5 Flow Cytometry

Kidney grafts were harvested, minced into small fragments, and digested in DMEM containing 1 mg/mL collagenase I and 0.1 mg/mL DNase I using an Octo Dissociator with Heaters. The digested tissue was passed through a 40-µm cell strainer to obtain a single-cell suspension. The collected cells were stained with Fixable Viability Dye eFluor 780 (1:1000, 65-0865-18, eBioscience, San Diego, CA, USA) to exclude dead cells and subsequently stained with fluorochrome-conjugated antibodies. Flow cytometric analysis was performed using a Beckman Coulter CytoFLEX flow cytometer and CytExpert software version 2.4.0 (Beckman Coulter, Brea, CA, USA). Fluorescein isothiocyanate-conjugated anti-mouse inducible nitric oxide synthase (iNOS) (1:50, 130-116-421, Miltenyi Biotec, Bergisch Gladbach, Germany) was used to identify M1 macrophages, allophycocyanin-conjugated anti-mouse CD206 (1:100, 17-2061-82, eBioscience) was used to identify M2 macrophages, and phycoerythrin-conjugated anti-mouse F4/80 (1:100, 12-4801-82, eBioscience, San Diego, CA, USA) was used to identify macrophages, according to the manufacturers' instructions.

2.6 RNA-Seq Analysis

Total RNA was extracted using the FastPure Cell/Tissue Total RNA Isolation Kit V2 (RC112-01, Vazyme). RNA sequencing was performed by Beijing Novogene Co., Ltd. according to the standard Illumina protocol. Differentially expressed genes (DEGs) were identified using R software 4.4.3 (R Foundation for Statistical Computing, Vienna, Austria). DEGs were selected using cutoff values of an absolute log fold change >0.5 and $p < 0.05$. The complete list of DEGs is provided in **Supplementary File 1**.

2.7 Real-Time Quantitative Polymerase Chain Reaction (RT-qPCR) Analysis

Total RNA was extracted using the FastPure Cell/Tissue Total RNA Isolation Kit V2 and reverse-transcribed into complementary DNA using HiScript III All-in-One RT SuperMix Perfect for qPCR (R333-01, Vazyme). Messenger RNA expression was quantified using ChamQ SYBR qPCR Master Mix (High ROX Premixed; Q341, Vazyme) on a StepOnePlus Real-Time PCR System (Applied Biosystems). Messenger RNA expression levels were normalized to β-actin and calculated using the $2^{-\Delta\Delta Ct}$ method. Data are presented as the mean ± standard deviation (SD) of at least three independent experiments.

2.8 Western Blotting (WB)

Proteins were extracted from macrophages using radioimmunoprecipitation assay lysis buffer supplemented with a complete protease inhibitor cocktail and phenylmethylsulfonyl fluoride. WB was performed according to standard protocols. The following primary antibodies were used: anti-NOTCH4 (1:1000, TA379234, OriGene, Rockville, MD, USA), anti-Jagged Canonical Notch Ligand 1 (Jagged1) (1:1000, 70109, Cell Signaling Technology, Danvers, MA, USA), anti-iNOS (1:1000, 13120, Cell Signaling Technology, Danvers, MA, USA), anti-HES1 (1:1000, R381205, Zenbio, Research Triangle Park, NC, USA), anti-Hes Related Family bHLH Transcription Factor with YRPW Motif 1 (HEY1) (1:1000, 19929-1-AP, Proteintech group, Wuhan, Hubei, China), anti-KLF4 (1:1000, 11880-1-AP, Proteintech group, Wuhan, Hubei, China), and anti-Glyceraldehyde-3-phosphate Dehydrogenase (GAPDH) (1:5000, 60004-1-Ig, Proteintech group, Wuhan, Hubei, China).

2.9 Chromatin Immunoprecipitation (ChIP)—PCR

ChIP was carried out with a commercial ChIP assay kit (P2080S, Beyotime Biotechnology, Shanghai, China) following the manufacturer's protocols. In short, cells (1×10^6 cells) were fixed via crosslinking in 1% formaldehyde solution at 37 °C for 10 min, and glycine was supplemented to terminate the crosslinking reaction. Cells were rinsed using pre-cooled PBS (G4200, Servicebio, Wuhan, Hubei, China) containing 1 mM phenylmethanesulfonyl fluoride (ST505, Beyotime Biotechnology, Shanghai, China), followed by centrifugation and lysis in sodium dodecyl sulfate lysis buffer supplemented with 1 mM PMSF. Chromatin fragments ranging from 200 to 500 bp were generated by sonication: 10 cycles of 10-second sonication separated by 10-second cooling intervals. Cell lysates were incubated overnight at 4 °C with either control IgG (A7016, Beyotime Biotechnology, Shanghai, China) or anti-HES1 antibody. Afterwards, Protein A+G Agarose coupled with Salmon Sperm DNA was added and incubated at 4 °C for 3 h. Sequential washes with low-salt and high-salt buffers, DNA elution and reverse crosslinking were performed subsequently. Purification of immunoprecipitated DNA was conducted after treatment with ethylenediaminetetraacetic acid (C0196, Beyotime Biotechnology, Shanghai, China), Tris (pH 6.5) and proteinase K at 45 °C for 1 h, and the recovered DNA was subjected to PCR.

2.10 Statistical Analysis

All experiments were independently repeated at least three times, and data are expressed as the mean ± SD. Comparisons among multiple groups were performed using one-way analysis of variance followed by Tukey's post hoc test. Differences between two groups were evaluated using a nonparametric test because of the limited sample size. A two-sided p value < 0.05 was considered statistically significant.

3. Results

3.1 M1 Macrophages Exhibit Significant Infiltration in ABMR Allografts

A mouse model of allogeneic ABMR was established through skin graft-mediated presensitization followed by heterotopic kidney transplantation. H&E and PAS staining showed that, compared with the SYN group, the ABMR group exhibited marked acute tubular injury, peritubular capillaritis, and glomerulitis, consistent with the characteristic pathological features of acute antibody-mediated renal allograft injury (Fig. 1A,B). IF staining of the renal allografts from ABMR mice revealed linear C3d deposition in the peritubular capillaries (Fig. 1C,D). These findings confirmed the successful establishment of an allogeneic mouse model of renal transplant ABMR.

Immunohistochemical (IHC) staining for the macrophage marker F4/80 was performed on renal allograft tissues from mice in the SYN and ABMR groups. The number of F4/80-positive cells in the renal interstitium was markedly higher in the ABMR group than in the SYN group, with extensive macrophage infiltration throughout the allograft interstitium (Fig. 1E,F). Analysis of iNOS, a marker of M1 macrophages, and CD206, a marker of M2 macrophages, within F4/80-positive cells revealed a marked increase in the number of iNOS-positive macrophages infiltrating the renal interstitium of ABMR mice. In contrast, the number of CD206-positive cells did not differ significantly, indicating substantial M1 macrophage infiltration into the renal interstitium of kidney allografts affected by ABMR (Fig. 1G–I). Dual IF staining for F4/80 and iNOS was also performed on renal allograft tissues from the SYN and ABMR groups. The number of F4/80- and iNOS-double-positive cells in the renal interstitium was markedly higher in the ABMR group than in the SYN group (Fig. 1J). Similar findings were identified in human specimens in our previous study [8].

3.2 IGT Inhibits ABMR Progression and Reduces M1 Macrophage Infiltration in a Mouse Model of ABMR

Mice were treated with IGT at 35 mg/kg/day by oral gavage. H&E and PAS staining showed that, compared with the ABMR group, the IGT-treated group exhibited markedly reduced peritubular capillaritis and mononuclear cell infiltration within large vessels, together with alleviation of arteritis and venulitis (Fig. 2A,B). Concurrently, C3d deposition in the grafts was significantly reduced following IGT treatment (Fig. 2C,D). These findings indicate that IGT substantially attenuates the characteristic pathological manifestations of ABMR-associated renal allograft injury. F4/80 IHC staining was performed on renal allograft tissues from mice in each group. F4/80-positive staining in the renal interstitium was markedly reduced in the ABMR+IGT group compared with the ABMR group (Fig. 2E,F). Single-cell suspensions were prepared from the renal allografts of mice in each group and analysed by flow cytometry. After gating on F4/80-positive macrophages, the expression of iNOS and CD206 was assessed. The proportion of iNOS-positive cells was markedly reduced in the IGT group, whereas the proportion of CD206-positive cells did not change significantly (Fig. 2G–I). Dual IF staining for F4/80 and iNOS in renal allografts from the ABMR and IGT groups yielded results consistent with the flow cytometric findings (Fig. 2J). These results suggest that IGT reduces M1 macrophage infiltration into the renal interstitium of transplanted kidneys.

3.3 IGT Inhibits M1 Macrophage Polarization In Vitro

To further validate the effects of IGT on macrophage polarization, BMDMs were isolated for *in vitro* experiments. The mRNA expression levels of iNOS, CD86, tumor necrosis factor alpha (TNF-α), and interleukin-1 beta (IL-1β) were significantly lower in the M1+IGT group than in the M1 group (Fig. 3A–D). WB showed that iNOS protein expression was markedly reduced in BMDMs from the M1+IGT group compared with those from the M1 group (Fig. 3E,F). Dual IF staining for F4/80 and iNOS further revealed a marked reduction in the number of F4/80- and iNOS-double-positive cells in the M1+IGT group compared with the M1 group (Fig. 3G).

3.4 IGT Alters the JAG1-NOTCH4 Pathway in M1 Macrophages

To further investigate the mechanism underlying the effects of IGT, RNA was extracted from BMDMs following IGT treatment and subjected to transcriptomic sequencing. A total of 7343 DEGs were identified between the M1 and M0 groups, whereas 163 DEGs were identified between the M1+IGT and M1 groups (Fig. 4A,B). Intersection analysis of the DEGs identified in these two comparisons revealed 134 genes that may be involved in the IGT-mediated inhibition of M1 macrophage polarization (Fig. 4C). After excluding genes that were also differentially expressed between the M1 and M0 groups, we selected the 15 most significantly altered genes from the M1+IGT versus M1 comparison (**Supplementary File 2-Supplementary Table 1**). Among these genes, inflammation-related genes, including endothelin receptor type B (*EDNRB*), hepatitis A virus cellular receptor 2 (*HAVCR2*), thrombospondin-1 (*THBS1*), and *NOTCH4*, were subsequently validated using RT-qPCR and WB (**Supplementary File 2-Supplementary Fig. 1**). RT-qPCR analysis showed no significant changes in EDNRB or HAVCR2 expression, whereas WB revealed no apparent alteration in THBS1 protein expression. Transcriptomic analysis indicated a significant alteration in NOTCH4 transcription following IGT treatment, whereas changes in the expression of other components of the NOTCH pathway remained unclear. RT-qPCR analysis of NOTCH pathway components in the M1 and M1+IGT groups demonstrated substantial reductions in the mRNA expression of both the ligand Jagged1 and the receptor NOTCH4 following IGT

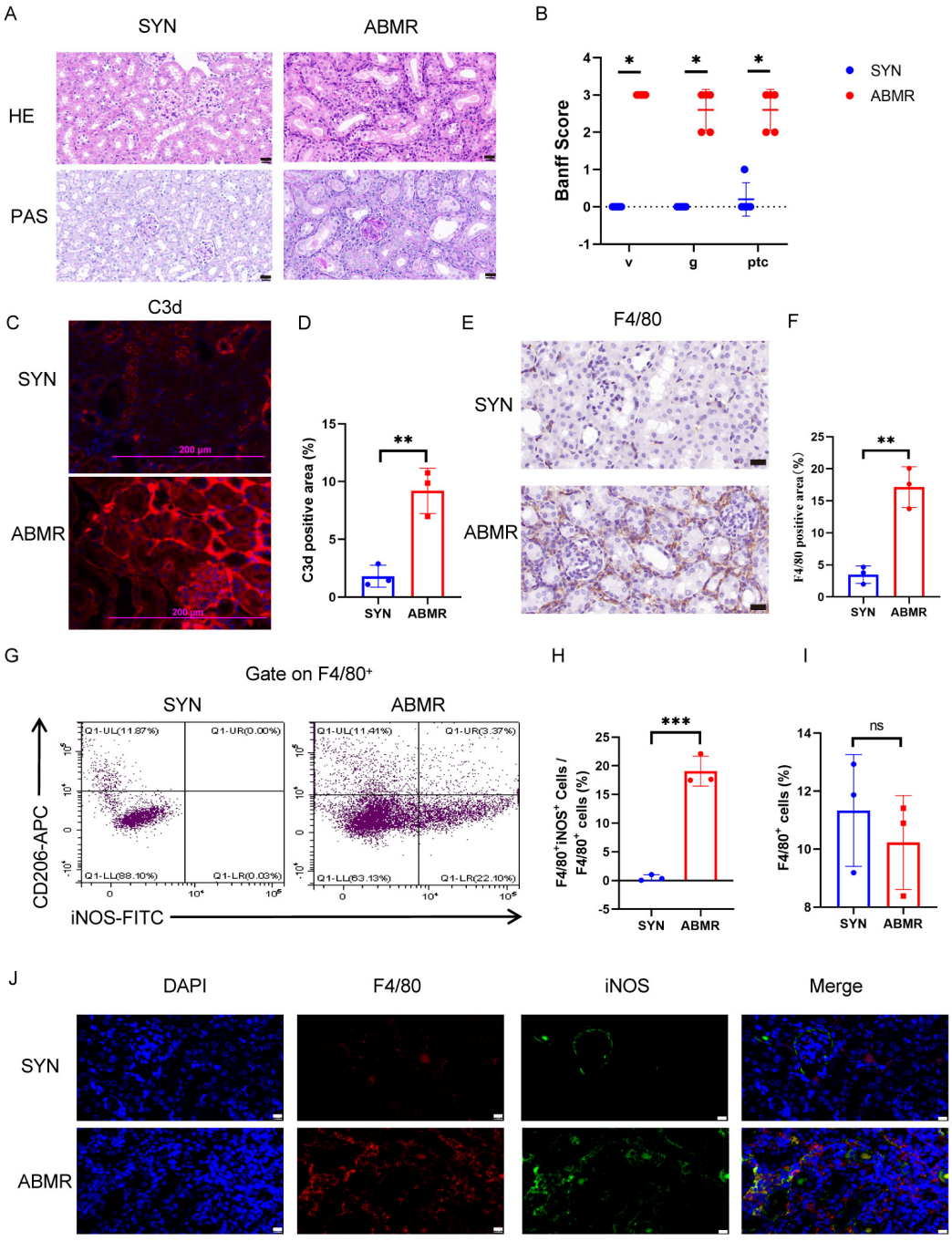


Fig. 1. Significant infiltration of M1 macrophages in ABMR allografts. Five days after skin transplantation, C57BL/6 recipient mice underwent kidney transplantation with grafts obtained from either C57BL/6 donors as SYN grafts or BALB/c donors as allografts. The recipient mice were euthanized on postoperative day 5. (A) Representative histological images of graft sections stained with H&E or PAS. Original magnification, ×400; scale bar, 20 μm. n = 5. (B) Banff scores for vasculitis, glomerulitis, and peritubular capillaritis in the grafts. n = 5. (C,D) Representative IF images and quantitative analysis of C3d deposition in the grafts. Original magnification, ×400; scale bar, 200 μm; n = 3. (E,F) Representative IHC images and quantitative analysis of F4/80 expression in the grafts. Original magnification, ×400; scale bar, 20 μm; n = 3. (G–I) Flow cytometric analysis of the proportions of $F4/80^{+}iNOS^{+}$ M1 macrophages and $F4/80^{+}CD206^{+}$ M2 macrophages in the grafts. n = 3. (J) Representative IF staining for F4/80 and iNOS in the grafts. Original magnification, ×400; scale bar, 20 μm; n = 3. ns, $p > 0.05$; * $p < 0.05$; ** $p < 0.01$; *** $p < 0.001$. ABMR, antibody-mediated rejection; SYN, Syngeneic; H&E, hematoxylin and eosin; PAS, periodic acid-Schiff; IF, immunofluorescence; IHC, immunohistochemistry; iNOS, inducible nitric oxide synthase.

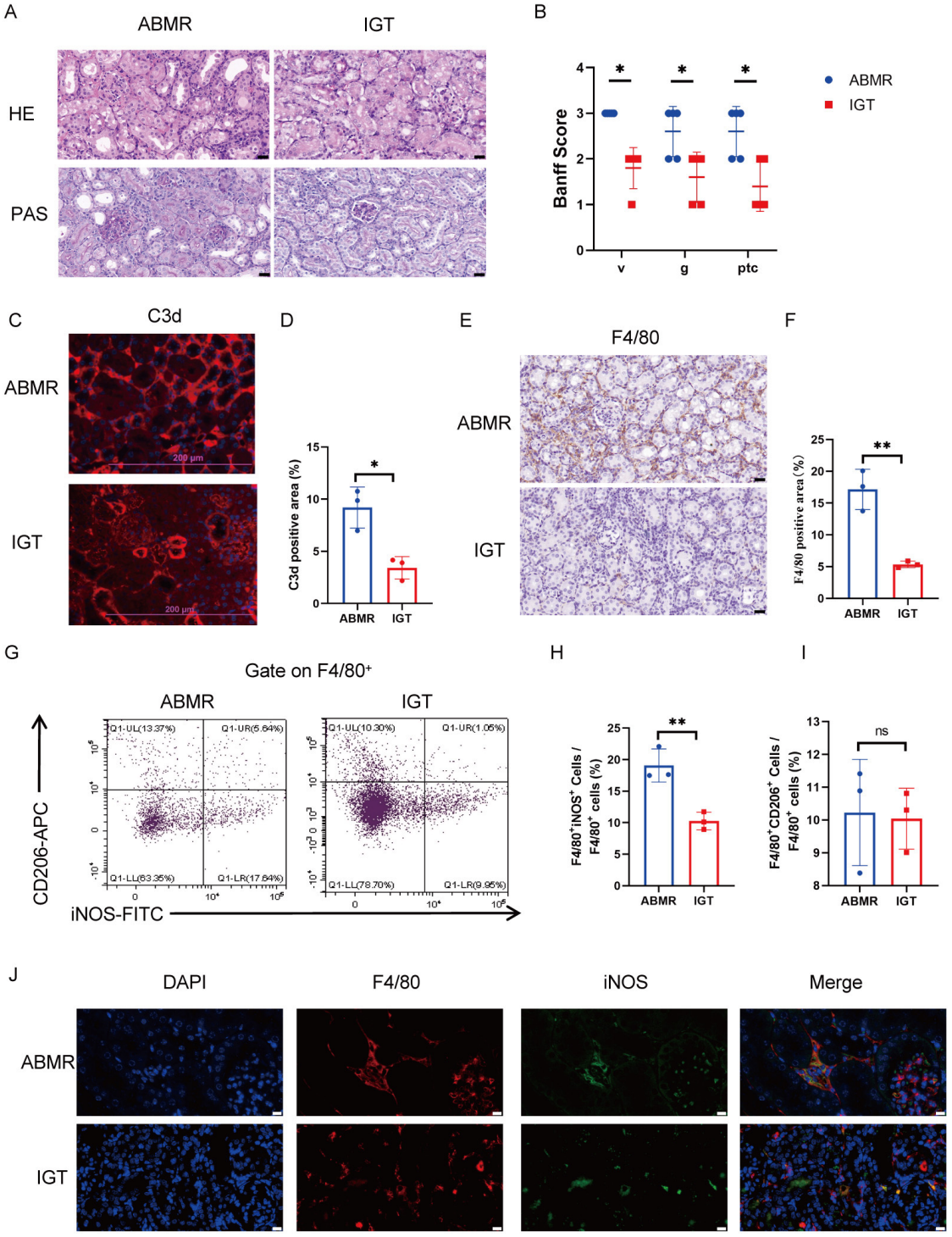


Fig. 2. IGT inhibits ABMR progression and reduces M1 macrophage infiltration in a mouse model of ABMR. Oral administration of IGT at 35 mg/kg/day was initiated on the day of skin graft-mediated sensitization. (A) Representative histological images of graft sections stained with H&E and PAS. Original magnification, ×400; scale bar, 20 μm; n = 5. (B) Banff scores for vasculitis, glomerulitis, and peritubular capillaritis in the grafts. n = 5. (C,D) Representative IF images and quantitative analysis of C3d deposition in the grafts. Original magnification, ×400; scale bar, 200 μm; n = 3. (E,F) Representative IHC images and quantitative analysis of F4/80 expression in the grafts. Original magnification, ×400; scale bar, 20 μm; n = 3. (G–I) Flow cytometric analysis of the proportions of $F4/80^{+}iNOS^{+}$ M1 macrophages and $F4/80^{+}CD206^{+}$ M2 macrophages in the grafts. n = 3. (J) Representative IF staining for F4/80 and iNOS in the grafts. Original magnification, ×400; scale bar, 20 μm; n = 3. ns, $p > 0.05$; * $p < 0.05$; ** $p < 0.01$. IGT, iguratimod.

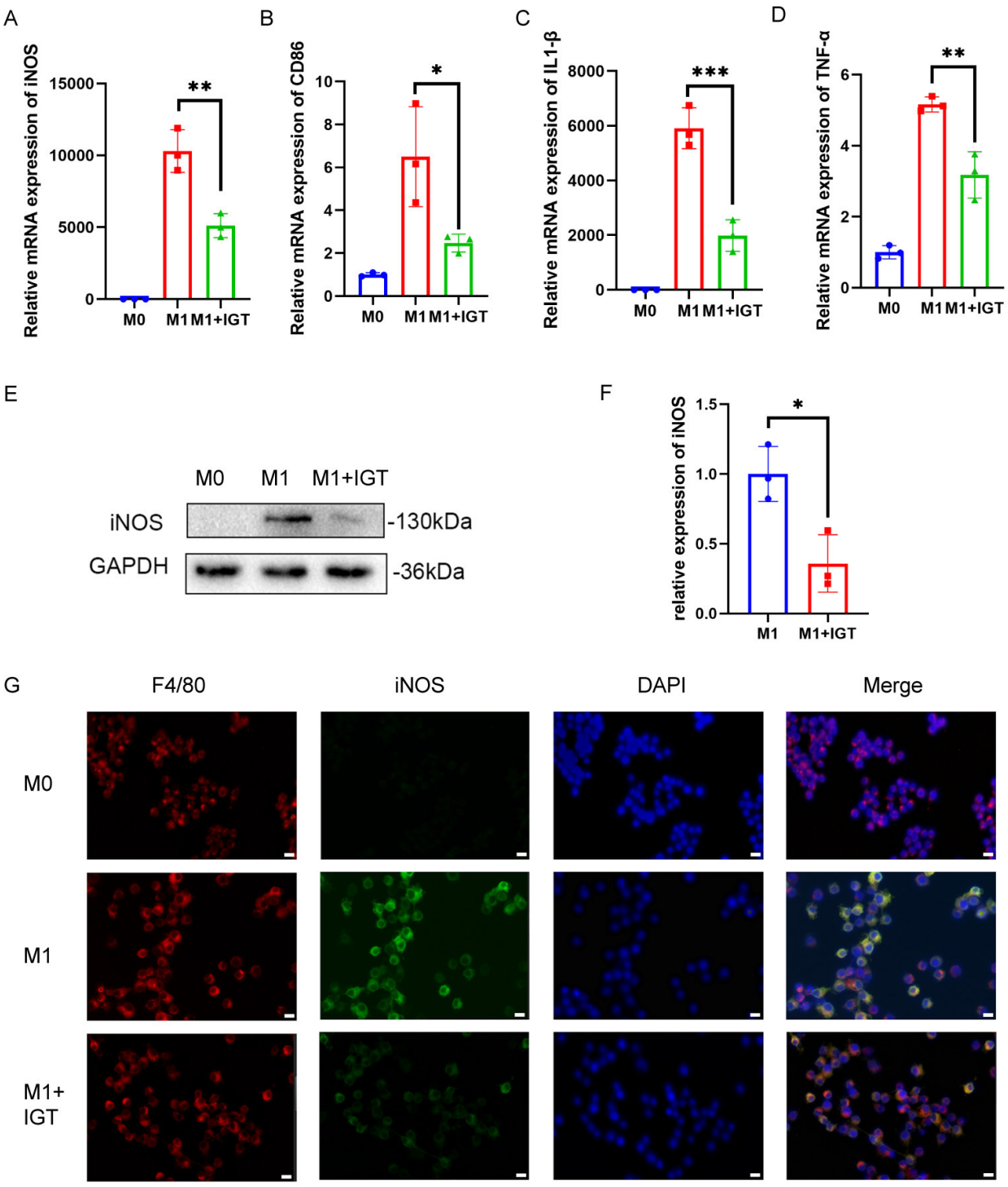


Fig. 3. IGT inhibits M1 macrophage polarization *in vitro*. (A–D) RT-qPCR analysis of the mRNA expression levels of iNOS (A), CD86 (B), IL-1β (C), and TNF-α (D) in BMDMs following IGT treatment. n = 3. (E,F) Representative WB and quantitative analysis showing reduced iNOS protein expression in BMDMs following IGT treatment. n = 3. (G) Representative IF staining showing reduced numbers of F4/80^{+}iNOS^{+} M1 macrophages among BMDMs following IGT treatment. Original magnification, ×400; scale bar, 20 μm; n = 3. * $p < 0.05$; ** $p < 0.01$; *** $p < 0.001$. RT-qPCR, real-time quantitative polymerase chain reaction; IL-1β, interleukin-1 beta; TNF-α, tumor necrosis factor alpha; BMDMs, bone marrow-derived macrophages; WB, Western blotting.

treatment. In contrast, the mRNA expression levels of other receptors, including NOTCH1, NOTCH2, and NOTCH3, did not differ significantly between the M1 and M1+IGT groups (Fig. 4D–H). Consistent with the RT-qPCR results,

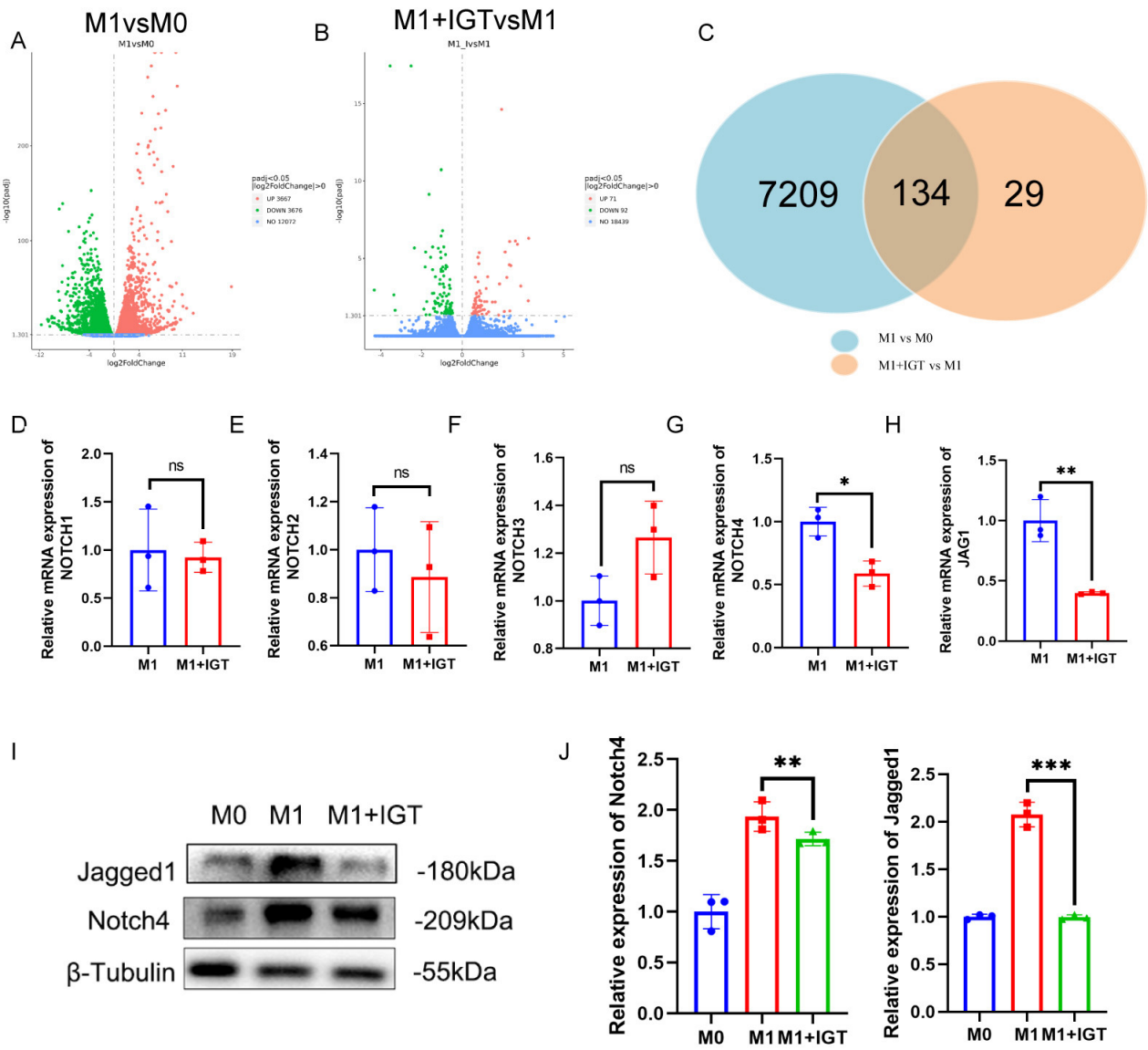


Fig. 4. IGT alters the Jagged1—NOTCH4 pathway in M1 macrophages. (A) Volcano plot showing DEGs between the M0 and M1 groups. n = 3. (B) Volcano plot showing DEGs between the M1 and M1+IGT groups. n = 3. (C) Venn diagram showing the genes shared between the two sets of DEGs. (D–H) RT-qPCR analysis of the mRNA expression levels of NOTCH1 (D), NOTCH2 (E), NOTCH3 (F), NOTCH4 (G), and JAG1 (H) in BMDMs following IGT treatment. n = 3. (I,J) Representative WB and quantitative analysis showing reduced NOTCH4 and Jagged1 protein expression in BMDMs following IGT treatment. n = 3. ns, $p > 0.05$; * $p < 0.05$; ** $p < 0.01$; *** $p < 0.001$. DEGs, differentially expressed genes; JAG1, Jagged Canonical Notch Ligand 1.

WB showed that JAGGED1 and NOTCH4 protein expression was significantly reduced in M1+IGT cells (Fig. 4I,J).

3.5 IGT Inhibits M1 Macrophage Polarization by Targeting the JAG1–NOTCH4 Pathway

Because NOTCH4 signaling requires receptor cleavage and the release of the NOTCH4 intracellular domain (N4ICD), we examined changes in N4ICD expression following IGT treatment. N4ICD expression was significantly reduced in response to IGT treatment (Fig. 5A,B). siRNA-mediated knockdown of NOTCH4 was subsequently used to inhibit the NOTCH pathway. NOTCH4 knockdown significantly reduced N4ICD generation in BMDMs, consistent with the effects of IGT treatment. Concurrently, inhibition of the NOTCH pathway reduced the expression of the M1 macrophage marker iNOS (Fig. 5C,D). The effects of N4ICD overexpression on iNOS expression were subsequently examined in macrophages. iNOS remained undetectable in both the M0 and M0+IGT groups, whereas iNOS expression was markedly elevated in N4ICD-overexpressing M1 macrophages compared with control M1 macrophages. Following IGT treatment, the re-

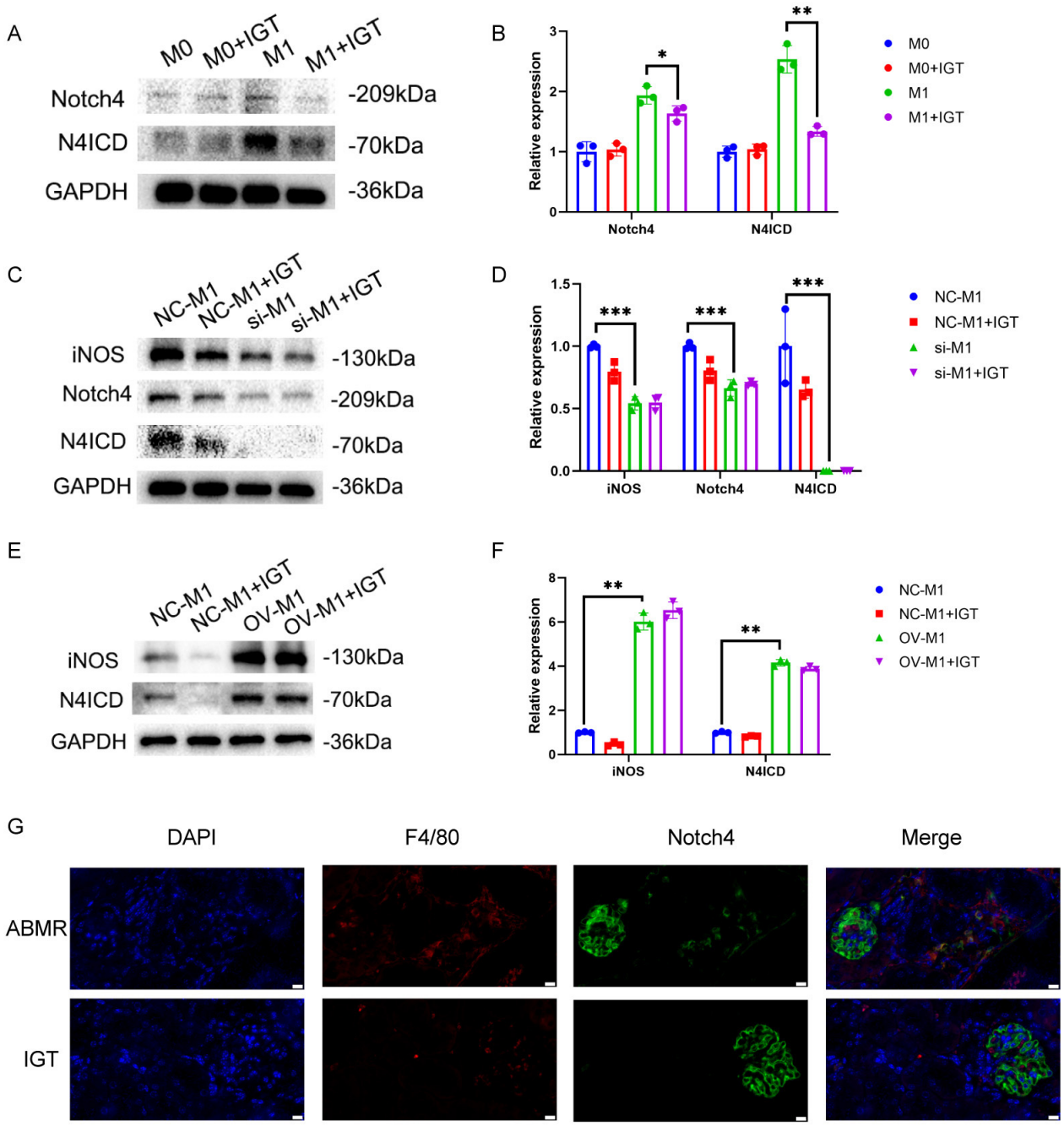


Fig. 5. IGT inhibits M1 macrophage polarization by targeting the JAG1–NOTCH4 pathway. (A,B) Representative WB and quantitative analysis of NOTCH4 and N4ICD expression in BMDMs following IGT treatment. (C,D) WB analysis of iNOS, NOTCH4, and N4ICD expression in macrophages following NOTCH4 knockdown. (E,F) WB analysis of iNOS and N4ICD expression in macrophages following N4ICD overexpression. (G) Representative IF staining for F4/80 and NOTCH4 in grafts following IGT treatment. Original magnification, ×400; scale bar, 20 μm; n = 3. * $p < 0.05$; ** $p < 0.01$; *** $p < 0.001$. N4ICD, NOTCH4 intracellular domain.

duction in iNOS expression was less pronounced in N4ICD-overexpressing macrophages than in control macrophages (Fig. 5E,F). IF staining further confirmed that IGT reduced NOTCH4 expression in macrophages (Fig. 5G).

3.6 NOTCH4 Deficiency Alleviates ABMR and Reduces M1 Macrophage Infiltration

To further validate the role of NOTCH4 in macrophage polarization and ABMR progression, an ABMR model was established using *NOTCH4*-knockout mice as recipients. Mouse genotypes were confirmed by extracting genomic DNA from tail-tip samples

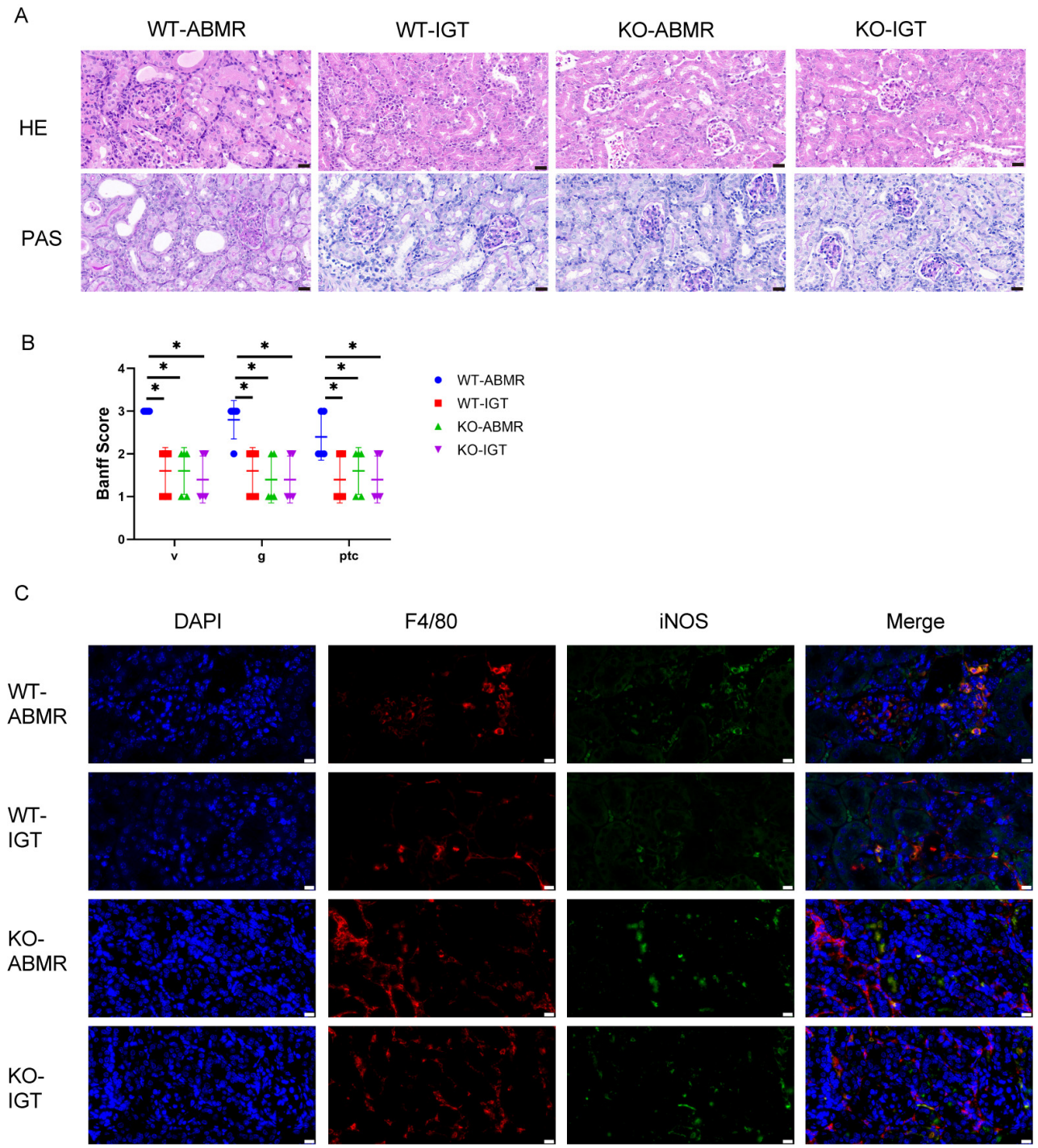


Fig. 6. NOTCH4 deficiency alleviates ABMR and reduces M1 macrophage infiltration. (A) Representative histological images of graft sections stained with H&E and PAS. Original magnification, ×400; scale bar, 20 µm; n = 5. (B) Banff scores for vasculitis, glomerulitis, and peritubular capillaritis in the grafts. n = 5. (C) Representative IF staining for F4/80 and iNOS in the grafts. Original magnification, ×400; scale bar, 20 µm; n = 3. * $p < 0.05$.

(**Supplementary File 2-Supplementary Fig. 2**). Histological examination using H&E and PAS staining revealed reduced mononuclear cell infiltration in the renal interstitium of grafts transplanted into NOTCH4-knockout mice. Acute tubular injury was attenuated, accompanied by markedly reduced peritubular capillaritis and significantly decreased mononuclear cell infiltration within large vessels. Arterial and venous inflammation was also substantially less pronounced than that in the ABMR group (Fig. 6A,B). IF analysis further demonstrated that NOTCH4 deficiency reduced M1 macrophage polarization (Fig. 6C).

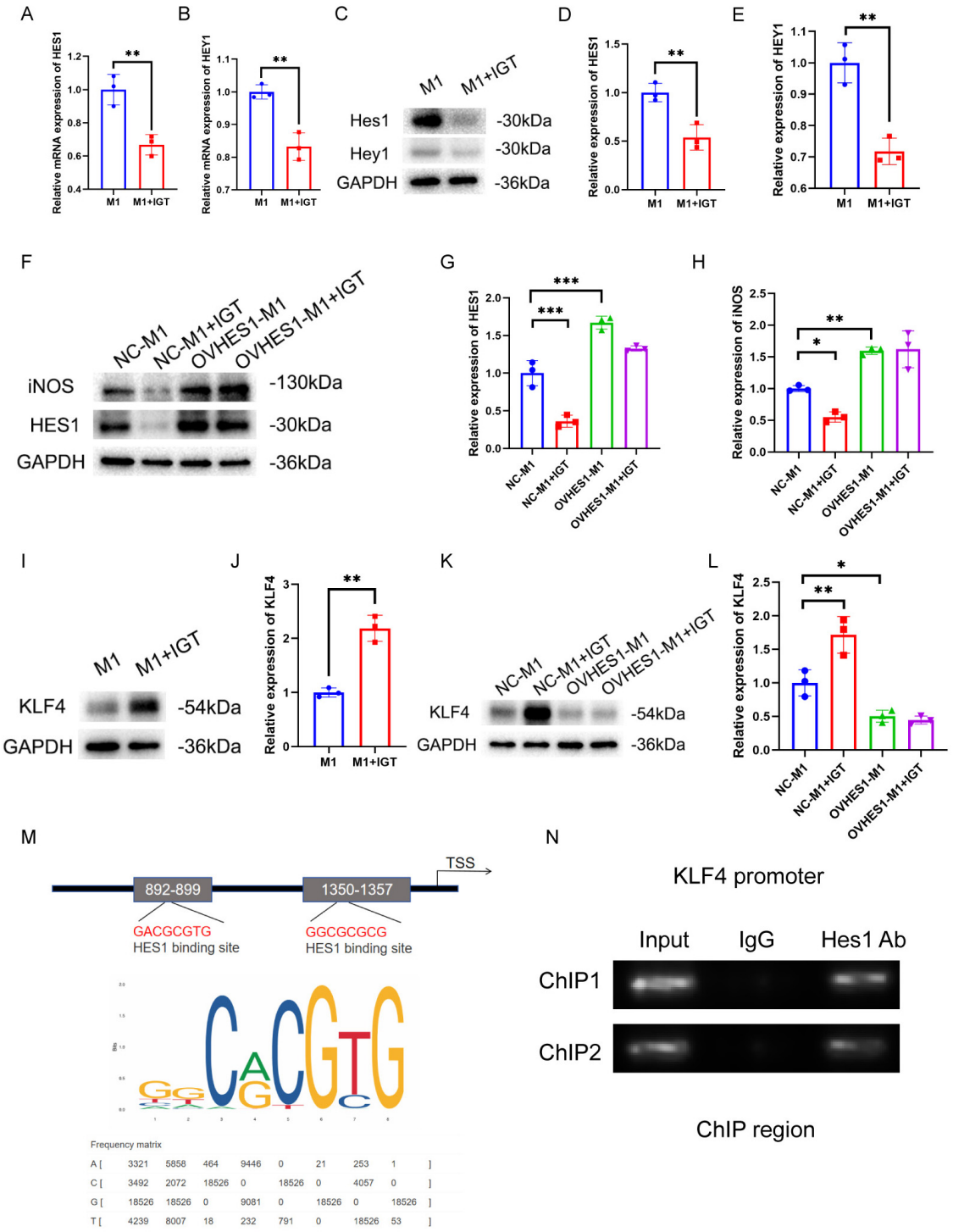


Fig. 7. IGT promotes KLF4 expression by inhibiting N4ICD/HES1 signaling. (A,B) RT-qPCR analysis of the mRNA expression levels of HES1 (A) and HEY1 (B) in BMDMs following IGT treatment. n = 3. (C–E) Representative WB and quantitative analysis of HES1 and HEY1 protein expression in BMDMs following IGT treatment. n = 3. (F–H) WB analysis of iNOS and HES1 expression in macrophages following HES1 overexpression. n = 3. (I,J) Representative WB and quantitative analysis of KLF4 protein expression in BMDMs following IGT treatment. n = 3. (K,L) WB analysis of KLF4 expression in macrophages following HES1 overexpression. n = 3. (M) The HES1-binding motif was predicted by JASPAR, and schematic images of the potential HES1 binding sites in the KLF4 promoter region are shown. (N) ChIP-PCR analysis of HES1 binding on KLF4 promoter. * $p < 0.05$; ** $p < 0.01$; *** $p < 0.001$. HES1, Hairy and Enhancer of Split 1; HEY1, Hes Related Family bHLH Transcription Factor with YRPW Motif 1; KLF4, Krüppel-like Factor 4; ChIP, chromatin immunoprecipitation.

3.7 IGT Promotes KLF4 Expression by Inhibiting N4ICD/HES1 Signaling

To further investigate the effects of IGT on the NOTCH signaling pathway, we examined HES1 and HEY1, two downstream transcription factors activated by NOTCH4. RT-qPCR analysis showed that IGT significantly suppressed the transcription of both HES1 and HEY1 (Fig. 7A,B). Analysis of HES1 and HEY1 protein expression revealed a particularly pronounced reduction in HES1 expression (Fig. 7C–E). Following HES1 overexpression in macrophages, the expression of the M1 macrophage marker iNOS was markedly increased (Fig. 7F–H). Moreover, HES1 overexpression attenuated the inhibitory effect of IGT on M1 macrophage polarization, suggesting that HES1 acts downstream of IGT. To determine whether HES1 is also influenced by pathways other than the Notch pathway, we used JSH (3 μM) to inhibit the Nuclear factor kappa-light-chain-enhancer of activated B cells (NF-κB) pathway. The results showed that HES1 levels remained unchanged following inhibition of the NF-κB pathway, suggesting that HES1 is not influenced by the NF-κB pathway acting in isolation (**Supplementary File 2-Supplementary Fig. 3**).

Previous studies have demonstrated that KLF4 plays a critical role in M1 macrophage polarization. Our previous investigation also showed that IGT increased KLF4 expression in macrophages [18]. This finding was further confirmed by WB analysis of KLF4 protein expression (Fig. 7I,J). Because HES1 functions as a transcriptional repressor, we hypothesized that the IGT-induced alteration in KLF4 expression might be dependent on HES1. Accordingly, KLF4 expression was assessed following HES1 overexpression, revealing a marked reduction in KLF4 protein levels in HES1-overexpressing macrophages (Fig. 7K,L). These findings indicate that IGT may regulate M1 macrophage polarization through N4ICD/HES1 signaling, thereby modulating KLF4 expression.

We identified whether HES1 directly regulated KLF4 transcription. The prediction of HES1 binding sites in the KLF4 promoter region using the JASPAR website (http://jaspar.genereg.net/) revealed two putative motifs, which had high scores, in the KLF4 promoter (Fig. 7M). Further, ChIP-PCR confirmed that HES1 binds to both promoter sites (Fig. 7N).

4. Discussion

Macrophages play a critical role in maintaining immune microenvironmental homeostasis [21,22]. In this study, we observed substantial infiltration of M1 macrophages into renal allografts in a mouse model of ABMR. IGT treatment reduced M1 macrophage polarization and attenuated renal allograft injury. Our findings further suggest that the inhibitory effect of IGT on M1 macrophage polarization may be mediated through the NOTCH4/HES1/KLF4 axis.

The NOTCH signaling pathway participates in numerous biological processes, including cell-fate determination, embryonic and tissue development, tissue repair, and inflammatory responses [23]. Unlike many signaling pathways, NOTCH signaling does not involve a conventional intracellular cascade of intermediary molecules. Instead, the NOTCH receptor undergoes sequential proteolytic cleavage, resulting in the release of the NICD, which translocates directly to the nucleus and regulates target-gene transcription. Furthermore, S2 cleavage of the NOTCH receptor is initiated through its interaction with ligands expressed on neighboring cells. Consequently, NOTCH signaling acts over a relatively short range but elicits a rapid cellular response [24]. Previous studies have identified the NOTCH signaling pathway as an important regulator of $CD4^+$ T cells in graft-versus-host disease [25]. Inhibition of NOTCH signaling reduces target-organ injury and germinal-center formation, thereby markedly decreasing the severity and mortality of graft-versus-host disease. Conversely, activation of NOTCH signaling directly stimulates T cells and enhances their effector functions [26]. Further studies reveal that expression dynamics on regulatory T cells suppress dual-regulatory protein-dependent tissue repair, promoting severe pulmonary inflammation [27]. NOTCH4 activation also exacerbates nuclear factor-κB-mediated inflammation in human immunodeficiency virus-associated nephropathy [28]. Previous studies have confirmed that there is a certain degree of functional overlap between the Notch and NF-κB pathways. Another research on NOTCH4 has also proposed and validated a hypothesis that NICD4 upregulates HES1 expression by competitively binding to the HES1 promoter in opposition to p-STAT3 [29]. Furthermore, activation of NOTCH signaling markedly enhances B-cell receptor responsiveness [30]. Thus, the NOTCH signaling pathway plays critical roles in both adaptive and innate immunity by regulating the functions of multiple immune-cell populations [31]. Our *in vitro* experiments similarly demonstrated that NOTCH4 expression was elevated in M1 macrophages and that this increase was reversed by IGT treatment. We therefore hypothesize that NOTCH4 promotes inflammatory responses by enhancing M1 macrophage polarization.

Our group previously conducted clinical studies evaluating IGT in combination with conventional immunosuppressive regimens in kidney transplant recipients. The incidence of biopsy-proven acute rejection was significantly lower in the IGT group than in the control group, with no significant between-group differences in adverse reactions [16,17]. However, the immunosuppressive mechanisms of IGT remain unclear, limiting its broader clinical application. Previous studies have found that IGT could inhibit the M1 and M2 polarization of macrophages in pulmonary fibrosis [32]. In the present study, we found that IGT significantly attenuated the progression of ABMR following kidney transplantation, an effect associated with the targeted

inhibition of M1 macrophage polarization. These findings partially elucidate the mechanism by which IGT alleviates ABMR and provide a theoretical basis for its further clinical application in kidney transplantation.

Our research further supports a potential association between NOTCH4 and KLF4. Previous studies have demonstrated that the active intracellular domain of NOTCH1 suppresses KLF4 promoter activity in colorectal cancer cells [33]. Another study showed that NOTCH1 inhibits KLF4 expression in intestinal epithelial cells [34]. However, evidence supporting such an association in immune cells remains limited. Our study demonstrated that HES1, a downstream transcriptional repressor of NOTCH4, suppresses KLF4 expression.

HES1 is a popular research target in renal injury, especially in acute kidney injury and renal fibrosis. In ischemia reperfusion injury, HES1 expression is upregulated [35]. However, its role is complex. Some studies suggest it promotes inflammation and apoptosis, acting as a detrimental factor, while others indicate it can activate protective anti-inflammatory pathways [36,37,38,39]. Our study confirmed that HES1 is highly expressed in M1 macrophages infiltrating the ABMR kidneys.

This study has several limitations. First, the effects of NOTCH4 on macrophage polarization and ABMR were validated only in global knockout mice. Further *in vivo* validation using an ABMR model established in macrophage-specific NOTCH4-knockout mice would provide more compelling evidence. Second, the interactions between macrophages and endothelial cells, as well as the molecular mechanisms underlying these interactions, require further investigation.

In summary, findings from both the mouse model of ABMR and the *in vitro* experiments suggest that IGT may delay ABMR progression following kidney transplantation by inhibiting NOTCH4-mediated M1 macrophage polarization. This effect may be mediated through regulation of the NOTCH4/HES1/KLF4 axis. Elucidating the effects and mechanisms of IGT provides new insights into its further development and application in transplantation medicine.

5. Conclusion

Our study demonstrated that M1 macrophage polarization contributes to the initiation and progression of ABMR following kidney transplantation. IGT attenuates M1 macrophage polarization by inhibitingJagged1–NOTCH4 signaling. These findings expand the current understanding of the mechanisms underlying the effects of IGT and may provide new insights into the effective prevention and treatment of ABMR.

Availability of Data and Materials

The datasets generated during and analyszed during the current study are available from the corresponding authors on reasonable request.

Author Contributions

ZH: Writing – original draft, Methodology, Investigation, Formal analysis, Conceptualization. JZ: Writing – original draft, Investigation. CY: Writing – original draft, Formal analysis. MZ: Methodology, Investigation, Formal analysis. ZY: Methodology, Formal analysis. JX: Methodology, Formal analysis. MG: Writing – review & editing, Supervision, Methodology, Conceptualization. PH: Writing – review & editing, Supervision, Methodology, Conceptualization. All authors contributed to editorial changes in the manuscript. All authors read and approved the final manuscript. All authors have participated sufficiently in the work and agreed to be accountable for all aspects of the work.

Ethics Approval and Consent to Participate

All animal experiments were approved by the Institutional Animal Care and Use Committee, Nanjing Medical University (Approve Number: IACUC-2109025) and carried out in accordance with the ARRIVE 2.0 guidelines and the Guidelines for the Ethical Review of Laboratory Animal Welfare of China.

Acknowledgment

Not applicable.

Funding

This work was supported by the National Natural Science Foundation of China [grant numbers 82470790, 82170769, 81900684], Jiangsu Province Natural Science Foundation Program [grant number BK20191063].

Conflicts of Interest

The authors declare no conflicts of interest.

Supplementary Material

Supplementary material associated with this article can be found, in the online version, at https://doi.org/10.31083/FBL54785.

References

[1] Chaudhry D, Chaudhry A, Peracha J, Sharif A. Survival for waitlisted kidney failure patients receiving transplantation versus remaining on waiting list: systematic review and meta-analysis. BMJ (Clinical Research Ed.). 2022; 376: e068769. https://doi.org/10.1136/bmj-2021-068769

[2] Halloran PF, Famulski KS, Reeve J. Molecular assessment of disease states in kidney transplant biopsy samples. Nature Reviews. Nephrology. 2016; 12: 534–548. https://doi.org/10.1038/nrneph.2016.85

[3] Loupy A, Lefaucheur C. Antibody-Mediated Rejection of Solid-Organ Allografts. The New England Journal of Medicine. 2018; 379: 1150–1160. https://doi.org/10.1056/NEJMra1802677

[4] Lefaucheur C, Viglietti D, Bentlejewski C, Duong van Huyen JP, Vernerey D, Aubert O, et al. IgG Donor-Specific Anti-Human HLA Antibody Subclasses and Kidney Allograft Antibody-

Mediated Injury. Journal of the American Society of Nephrology: JASN. 2016; 27: 293–304. https://doi.org/10.1681/ASN.2014111120

[5] Kloc M, Uosef A, Kubiak JZ, Ghobrial RM. Macrophage Proinflammatory Responses to Microorganisms and Transplanted Organs. International Journal of Molecular Sciences. 2020; 21: 9669. https://doi.org/10.3390/ijms21249669

[6] Zhao Y, Chen S, Lan P, Wu C, Dou Y, Xiao X, et al. Macrophage subpopulations and their impact on chronic allograft rejection versus graft acceptance in a mouse heart transplant model. American Journal of Transplantation: Official Journal of the American Society of Transplantation and the American Society of Transplant Surgeons. 2018; 18: 604–616. https://doi.org/10.1111/ajt.14543

[7] Luo M, Zhao F, Cheng H, Su M, Wang Y. Macrophage polarization: an important role in inflammatory diseases. Frontiers in Immunology. 2024; 15: 1352946. https://doi.org/10.3389/fimmu.2024.1352946

[8] Ni B, Yang C, Zhang J, Hang Z, Zheng M, Feng D, et al. Rictor Ameliorates Acute Antibody-Mediated Rejection Following Kidney Transplantation by Suppressing Macrophage M1 Polarization Through p65-NLRP3 Axis. Advanced Science (Weinheim, Baden-Wurttemberg, Germany). 2025; 12: e17119. https://doi.org/10.1002/advs.202417119

[9] Liu J, Zheng B, Cui Q, Zhu Y, Chu L, Geng Z, et al. Single-Cell Spatial Transcriptomics Unveils Platelet-Fueled Cycling Macrophages for Kidney Fibrosis. Advanced Science. 2024; 11: e2308505. https://doi.org/10.1002/advs.202308505

[10] Hou C, Zhang XR, Wei J, Wang JN, Gao J, Wang ZJ, et al. METTL1-mediated m7G methylation of Sarm1 mRNA promotes macrophage inflammatory responses and multiple organ injury. Science Immunology. 2025; 10: eadv4810. https://doi.org/10.1126/sciimmunol.adv4810

[11] Wang Z, Gao X, Ji H, Shao M, Ni B, Fei S, et al. Characterization of gut microbiota and metabolites in renal transplant recipients during COVID-19 and prediction of one-year allograft function. Journal of Translational Medicine. 2025; 23: 420. https://doi.org/10.1186/s12967-025-06090-5

[12] Yuan JS, Kousis PC, Suliman S, Visan I, Guidos CJ. Functions of notch signaling in the immune system: consensus and controversies. Annual Review of Immunology. 2010; 28: 343–365. https://doi.org/10.1146/annurev.immunol.021908.132719

[13] Previs RA, Coleman RL, Harris AL, Sood AK. Molecular pathways: translational and therapeutic implications of the Notch signaling pathway in cancer. Clinical Cancer Research: an Official Journal of the American Association for Cancer Research. 2015; 21: 955–961. https://doi.org/10.1158/1078-0432.CCR-14-0809

[14] Mu R, Li C, Li X, Ke Y, Zhao L, Chen L, et al. Effectiveness and safety of iguratimod treatment in patients with active rheumatoid arthritis in Chinese: A nationwide, prospective real-world study. The Lancet Regional Health. Western Pacific. 2021; 10: 100128. https://doi.org/10.1016/j.lanwpc.2021.100128

[15] Xue L, Xu J, Lu W, Fu J, Liu Z. Iguratimod alleviates tubulointerstitial injury in mice with lupus. Renal Failure. 2022; 44: 636–647. https://doi.org/10.1080/0886022X.2022.2058962

[16] Feng D, Huang Z, Chen H, Tao J, Gao X, Liu J, et al. Iguratimod reduces panel reactive antibody in high mismatched renal transplant recipients: One single-center experience. Clinical Transplantation. 2022; 36: e14565. https://doi.org/10.1111/ctr.14565

[17] Tao J, Sun L, Wang Z, Chen H, Han Z, Zhang H, et al. Efficacy and Safety of Iguratimod Supplement to the Standard Immunosuppressive Regimen in Highly Mismatched Renal Transplant Recipients: A Pilot Study. Frontiers in Immunology. 2021; 12: 738392. https://doi.org/10.3389/fimmu.2021.738392

[18] Hang Z, Wei J, Zheng M, Gui Z, Chen H, Sun L, et al. Iguratimod Attenuates Macrophage Polarization and Antibody-Mediated Rejection After Renal Transplant by Regulating KLF4. Frontiers in Pharmacology. 2022; 13: 865363. https://doi.org/10.3389/fphar.2022.865363

[19] Loupy A, Haas M, Roufosse C, Naesens M, Adam B, Afrouzian M, et al. The Banff 2019 Kidney Meeting Report (I): Updates on and clarification of criteria for T cell- and antibody-mediated rejection. American Journal of Transplantation. 2020; 20: 2318–2331. https://doi.org/10.1111/ajt.15898

[20] Yu QQ, Yang ZX, Zhang JQ, Gui ZP, Ni B, Zheng M, et al. Establishment and characterization of a mouse model of chronic antibody-mediated rejection after allogeneic kidney transplantation [in Chinese]. Journal of Nanjing Medical University. 2025; 45: 1073–1081. https://doi.org/10.7655/NYDXBNSN250101

[21] Locati M, Curtale G, Mantovani A. Diversity, Mechanisms, and Significance of Macrophage Plasticity. Annual Review of Pathology. 2020; 15: 123–147. https://doi.org/10.1146/annurev-pathmechdis-012418-012718

[22] Meng XM, Wang L, Nikolic-Paterson DJ, Lan HY. Innate immune cells in acute and chronic kidney disease. Nature Reviews Nephrology. 2025; 21: 464–482. https://doi.org/10.1038/s41581-025-00958-x

[23] Kovall RA, Gebelein B, Sprinzak D, Kopan R. The Canonical Notch Signaling Pathway: Structural and Biochemical Insights into Shape, Sugar, and Force. Developmental Cell. 2017; 41: 228–241. https://doi.org/10.1016/j.devcel.2017.04.001

[24] Kopan R, Ilagan MXG. The canonical Notch signaling pathway: unfolding the activation mechanism. Cell. 2009; 137: 216–233. https://doi.org/10.1016/j.cell.2009.03.045

[25] Tkachev V, Vanderbeck A, Perkey E, Furlan SN, McGuckin C, Gómez Atria D, et al. Notch signaling drives intestinal graft-versus-host disease in mice and nonhuman primates. Science Translational Medicine. 2023; 15: eadd1175. https://doi.org/10.1126/scitranslmed.add1175

[26] Ferrandino F, Grazioli P, Bellavia D, Campese AF, Screpanti I, Felli MP. Notch and NF-κB: Coach and Players of Regulatory T-Cell Response in Cancer. Frontiers in Immunology. 2018; 9: 2165. https://doi.org/10.3389/fimmu.2018.02165

[27] Harb H, Benamar M, Lai PS, Contini P, Griffith JW, Crestani E, et al. Notch4 signaling limits regulatory T-cell-mediated tissue repair and promotes severe lung inflammation in viral infections. Immunity. 2021; 54: 1186–1199.e7. https://doi.org/10.1016/j.immuni.2021.04.002

[28] Puri RV, Yerrathota S, Home T, Idowu JY, Chakravarthi VP, Ward CJ, et al. Notch4 activation aggravates NF-κB-mediated inflammation in HIV-1-associated nephropathy. Disease Models & Mechanisms. 2019; 12: dmm040642. https://doi.org/10.1242/dmm.040642

[29] Zhang B, Dong S, Wang J, Huang T, Zhao P, Xu J, et al. NOTCH4$^{\Delta L12_16}$ sensitizes lung adenocarcinomas to EGFR-TKIs through transcriptional down-regulation of HES1. Nature Communications. 2023; 14: 3183. https://doi.org/10.1038/s41467-023-38833-7

[30] Poe JC, Jia W, Su H, Anand S, Rose JJ, Tata PV, et al. An aberrant NOTCH2-BCR signaling axis in B cells from patients with chronic GVHD. Blood. 2017; 130: 2131–2145. https://doi.org/10.1182/blood-2017-05-782466

[31] Zhang R, Du H, Liu Z, Lei Y, Hu H, Zheng J, et al. Macrophage Notch1 Participates in LPS-Induced Acute Lung Injury via Regulating CCR5 Expression in Mice. Frontiers in Bioscience (Landmark Edition). 2025; 30: 37430. https://doi.org/10.31083/FBL37430

[32] Xu H, Ma K, Ma Z, Zhuang T, Lin L. Iguratimod improves bleomycin-induced pulmonary inflammation and fibrosis by regulating macrophage polarization through inhibiting the TLR4/NF-κB pathway. Frontiers in Immunology. 2025; 16:

1558903. https://doi.org/10.3389/fimmu.2025.1558903
[33] Zheng H, Pritchard DM, Yang X, Bennett E, Liu G, Liu C, et al. KLF4 gene expression is inhibited by the notch signaling pathway that controls goblet cell differentiation in mouse gastrointestinal tract. American Journal of Physiology. Gastrointestinal and Liver Physiology. 2009; 296: G490–G498. https://doi.org/10.1152/ajpgi.90393.2008
[34] Ghaleb AM, Aggarwal G, Bialkowska AB, Nandan MO, Yang VW. Notch inhibits expression of the Krüppel-like factor 4 tumor suppressor in the intestinal epithelium. Molecular Cancer Research: MCR. 2008; 6: 1920–1927. https://doi.org/10.1158/1541-7786.MCR-08-0224
[35] Kobayashi T, Terada Y, Kuwana H, Tanaka H, Okado T, Kuwahara M, et al. Expression and function of the Delta-1/Notch-2/Hes-1 pathway during experimental acute kidney injury. Kidney International. 2008; 73: 1240–1250. https://doi.org/10.1038/ki.2008.74
[36] Elkhoely A. Liraglutide ameliorates gentamicin-induced acute kidney injury in rats via PGC-1α- mediated mitochondrial biogenesis: Involvement of PKA/CREB and Notch/Hes-1 signaling pathways. International Immunopharmacology. 2023; 114: 109578. https://doi.org/10.1016/j.intimp.2022.109578
[37] He Y, Xiao D, Zhu H, Chen C, Liu Q, Xie J, et al. Notch Signaling Aggravates Helicobacter pylori-Induced Inflammation by Promoting Macrophage Activation and Proinflammatory Th1/Th17 Responses. The American Journal of Pathology. 2025; 195: 1428–1442. https://doi.org/10.1016/j.ajpath.2025.04.007
[38] Chen Y, He Z, Zhao B, Zheng R. Downregulation of a potential therapeutic target NPAS2, regulated by p53, alleviates pulmonary fibrosis by inhibiting epithelial-mesenchymal transition via suppressing HES1. Cellular Signalling. 2023; 109: 110795. https://doi.org/10.1016/j.cellsig.2023.110795
[39] Pagie S, Gérard N, Charreau B. Notch signaling triggered via the ligand DLL4 impedes M2 macrophage differentiation and promotes their apoptosis. Cell Communication and Signaling. 2018; 16: 4. https://doi.org/10.1186/s12964-017-0214-x